Обзор ArXiv: astro-ph, 10-14 апреля 2017

От Сильченко О.К.

Astro-ph: 1704.02449

GROWTH OF BULGES IN DISC GALAXIES SINCE $Z \sim 1$

SONALI SACHDEVA AND KANAK SAHA
Inter-University Centre for Astronomy and Astrophysics, Pune 411007, India

AND

HARINDER P. SINGH
Department of Physics and Astrophysics, University of Delhi, Delhi 110007, India

Draft version April 11, 2017

ABSTRACT

We investigate the growth of bulges in bright ($M_B < -20$) disc galaxies since $z \sim 1$, in rest-frame B and I-band, using images from HST ACS and WFC3 in GOODS-South for high redshifts ($0.4 < z < 1.0$) and SDSS for local ($0.02 < z < 0.05$). The growth history has been traced by performing two-component bulge-disc decomposition and further classifying the bulges into pseudos and classicals using Kormendy relation. We have about 27% pseudo and 40% classical bulges in our

Три поля на разных z

TABLE 1
SAMPLE SIZE FOR DISC GALAXIES WITH PSEUDO AND CLASSICAL BULGES

Redshift	Rest frame	Discs with ($B/T > 0.1$)	Discs with pseudo bulges	Discs with classical bulges
0.77-1.0	*B*-band	175	64	111
0.77-1.0	*I*-band	141	48	93
0.4-0.77	*B*-band	140	62	78
0.4-0.77	*I*-band	109	44	65
0.02-0.05	*B*-band	64	27	37
0.02-0.05	*I*-band	59	24	35

Пример декомпозиции в двух полосах

B I B I

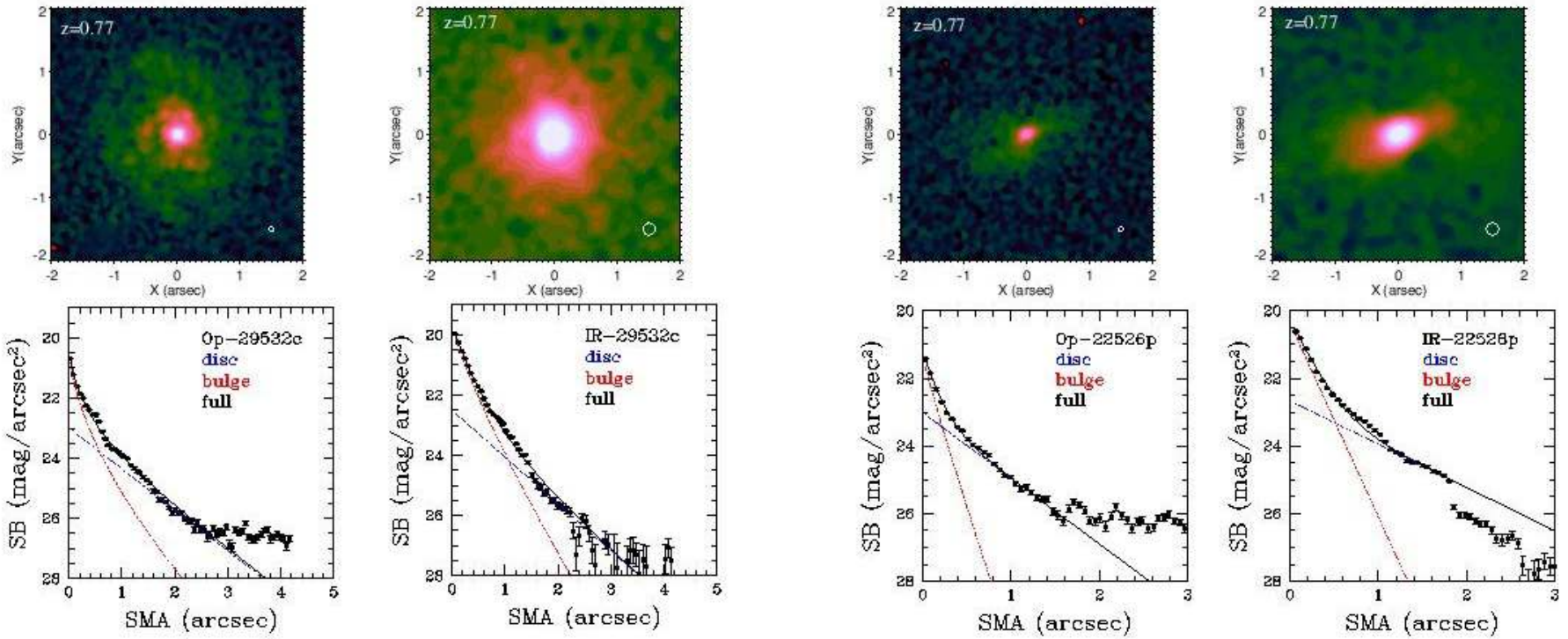

Классификация балджей на классические (внутри полосы Корменди) и псевдобалджи

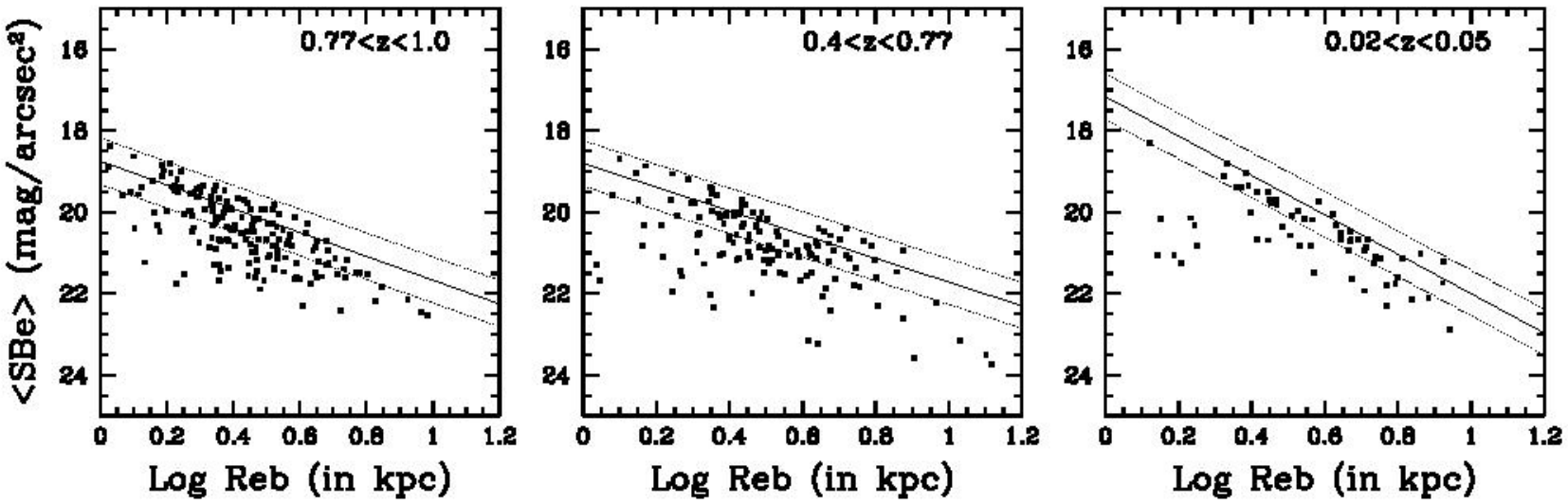

FIG. 2.— The solid line, in each of these three plots, depicts the Kormendy relation obtained for elliptical galaxies, in rest-frame B-band, in that redshift range. The dashed lines on the two sides of the solid line, represent the $\pm 3\sigma$ boundaries for a fixed slope. The dots refer to our sample of discs with bulges which have been placed according to their rest-frame B-band bulge parameters, i.e, average surface brightness and effective radius. Sources falling within the 3σ boundaries are identified as disc galaxies with classical bulges and those below are identified as discs with pseudo bulges.

Примеры классических балджей

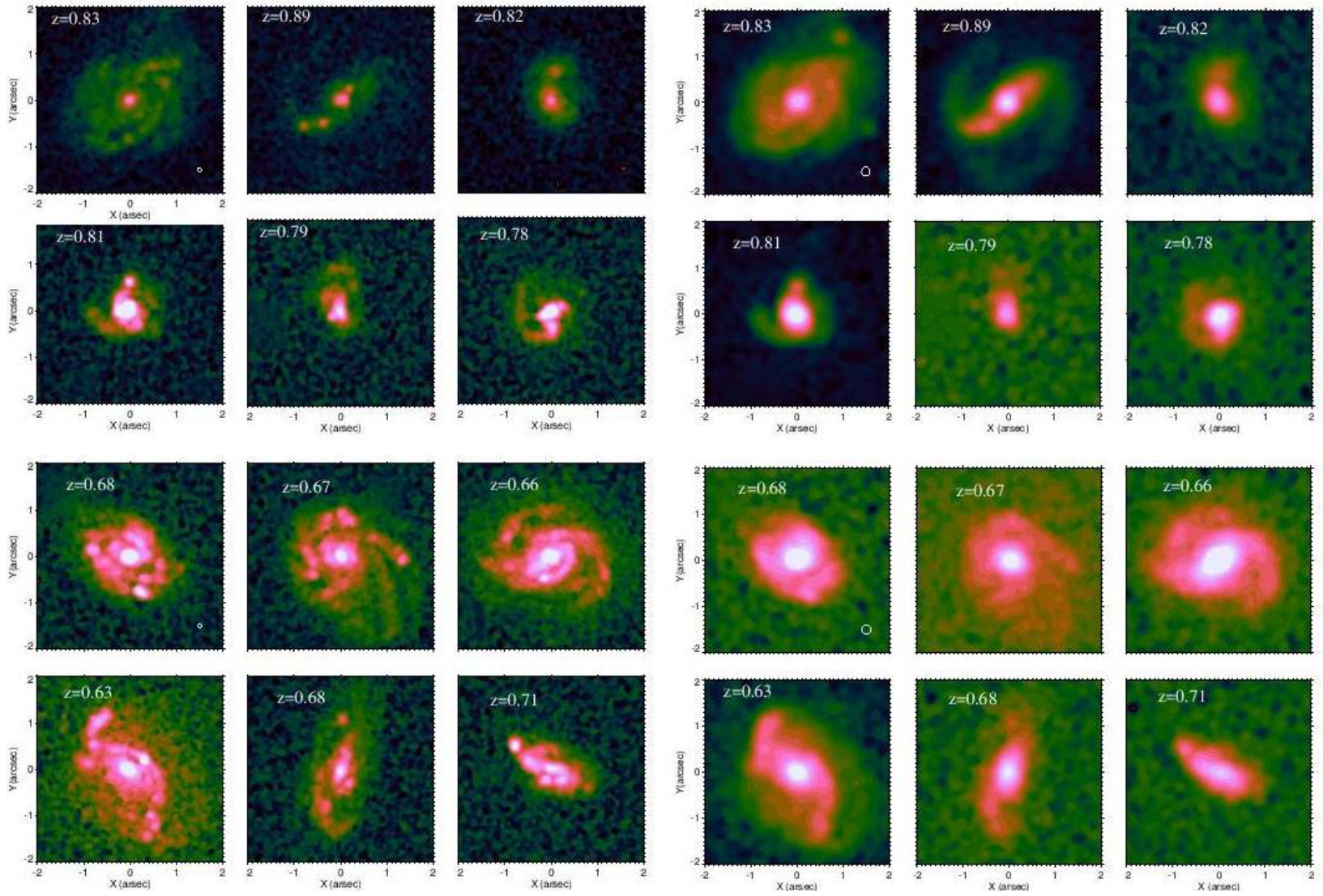

Примеры псевдобалджей

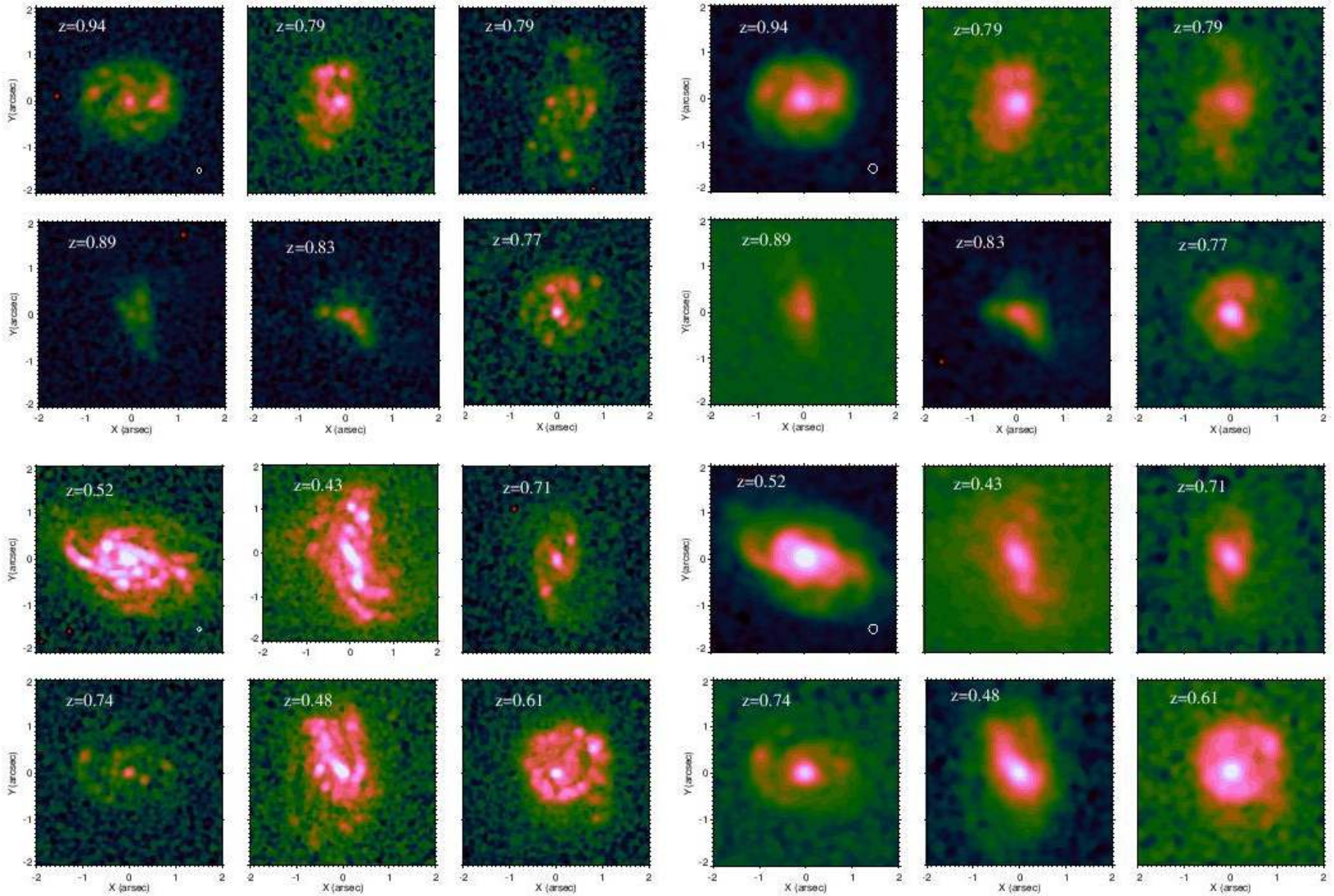

Медианные характеристики балджей

TABLE 2
PSEUDO BULGES IN REST-FRAME B AND I-BAND*

Redshift	R_e kpc	M_b mag	n_e	SB_e $mag/arcsec^2$	B/T	$Mass$ $(\times 10^{10})M_\odot$
Rest-frame B-band						
0.77-1.0	2.93(±0.72)	-19.77(±0.43)	0.93(±0.26)	21.83(±0.44)	0.102(±0.032)	0.06718(±0.05226)
0.4-0.77	3.14(±1.03)	-19.78(±0.45)	1.03(±0.24)	21.98(±0.45)	0.169(±0.081)	0.07078(±0.04368)
0.02-0.05	3.65(±1.94)	-20.38(±0.39)	1.11(±0.31)	21.78(±0.77)	0.255(±0.088)	0.42549(±0.15806)
Rest-frame I-band						
0.77-1.0	3.34(±0.68)	-21.03(±0.55)	0.86(±0.18)	21.01(±0.44)	0.496(±0.204)	0.35321(±0.25046)
0.4-0.77	3.33(±0.88)	-20.58(±0.82)	0.89(±0.21)	21.08(±0.67)	0.423(±0.156)	0.16609(±0.11083)
0.02-0.05	2.31(±0.77)	-21.10(±0.61)	1.21(±0.28)	19.96(±0.43)	0.178(±0.117)	0.37712(±0.18255)

*The values provided in the table are Median(±Median Absolute Deviation)

TABLE 3
CLASSICAL BULGES IN REST-FRAME B AND I-BAND*

Redshift	R_e kpc	M_b mag	n_e	SB_e $mag/arcsec^2$	B/T	$Mass$ $(\times 10^{10})M_\odot$
Rest-frame B-band						
0.77-1.0	2.41(±0.66)	-20.58(±0.28)	0.83(±0.15)	20.56(±0.50)	0.209(±0.038)	0.1331(±0.0776)
0.4-0.77	2.75(±0.79)	-20.64(±0.29)	0.91(±0.19)	20.82(±0.49)	0.372(±0.067)	0.2191(±0.1300)
0.02-0.05	3.84(±1.06)	-21.22(±0.13)	1.08(±0.13)	20.93(±0.57)	0.521(±0.106)	1.3502(±0.3394)
Rest-frame I-band						
0.77-1.0	2.60(±0.51)	-21.13(±0.56)	0.71(±0.14)	19.93(±0.41)	0.605(±0.171)	0.3991(±0.2506)
0.4-0.77	3.14(±0.82)	-21.43(±0.59)	0.77(±0.15)	20.09(±0.42)	0.632(±0.177)	0.3370(±0.1677)
0.02-0.05	2.21(±0.63)	-22.03(±0.53)	1.16(±0.22)	19.08(±0.39)	0.398(±0.123)	0.8842(±0.5761)

*The values provided in the table are Median(±Median Absolute Deviation)

Пример эволюции параметров – в данном случае, цвета

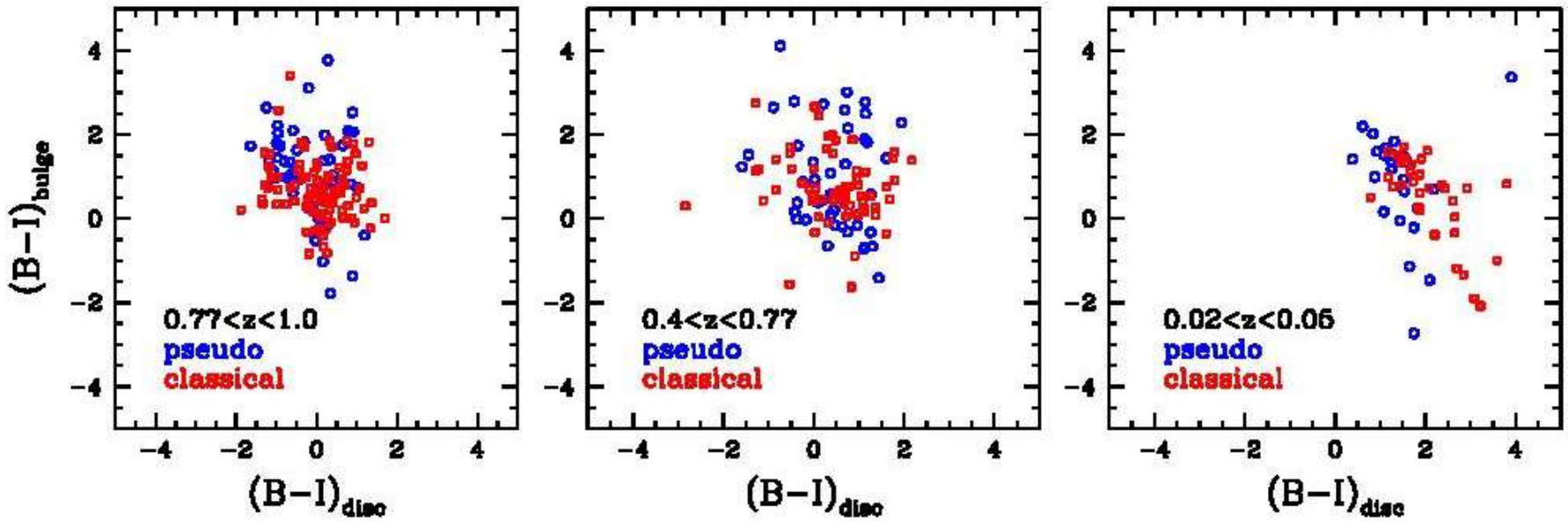

Весьма амбициозные и малоубедительные выводы

- Классические балджи растут за счет малого мержинга и аккреции;
- Псевдобалджи растут за счет секулярной эволюции – в добавлением аккреции?
- Почему-то (?) псевдобалджи компактифицируются со временем в фильтре I и растут в полосе B.

Astro-ph: 1704.03481

THE EDGE–CALIFA SURVEY: VARIATIONS IN THE MOLECULAR GAS DEPLETION TIME IN LOCAL GALAXIES

DYAS UTOMO[1], ALBERTO D. BOLATTO[2], TONY WONG[3], EVE C. OSTRIKER[4], LEO BLITZ[1], SEBASTIAN F. SANCHEZ[5], DARIO COLOMBO[6], ADAM K. LEROY[7], YIXIAN CAO[3], HELMUT DANNERBAUER[8], RUBEN GARCIA-BENITO[9], BERND HUSEMANN[10], VESELINA KALINOVA[6], REBECCA C. LEVY[2], DAMIAN MAST[11], ERIK ROSOLOWSKY[12], AND STUART N. VOGEL[2]

[1] Department of Astronomy, University of California, Berkeley, CA 94704, USA (email: dyas@berkeley.edu)
[2] Department of Astronomy, University of Maryland, College Park, MD 20642, USA
[3] Department of Astronomy, University of Illinois, Urbana, IL 61801, USA
[4] Department of Astrophysical Sciences, Princeton University, Princeton, NJ 08544, USA
[5] Instituto de Astronomía, Universidad Nacional Autónoma de México, A.P. 70-264, 04510 México, D.F., Mexico
[6] Max Planck Institute for Radio Astronomy, Auf dem Hügel 69, D-53121 Bonn, Germany
[7] Department of Astronomy, The Ohio State University, Columbus, OH 43210, USA
[8] Instituto de Astrofísica de Canarias, E-38205 La Laguna, Tenerife, Spain
[9] Instituto de Astrofísica de Andalucía, CSIC, E-18008 Granada, Spain
[10] European Southern Observatory, D-85748 Garching bei München, Germany
[11] Observatorio Astronómico de Córdoba, 5000 Córdoba, Córdoba, Argentina
[12] Department of Physics, University of Alberta, Edmonton, T6G 2E1, Canada

ABSTRACT

We present results from the EDGE survey, a spatially resolved CO(1–0) follow-up to CALIFA, an optical Integral Field Unit (IFU) survey of local galaxies. By combining the data products of EDGE and CALIFA, we study the variation of molecular gas depletion time ($\tau_{\rm dep}$) on kiloparsec scales in 52 galaxies. We divide

Пример данных для одной из галактик

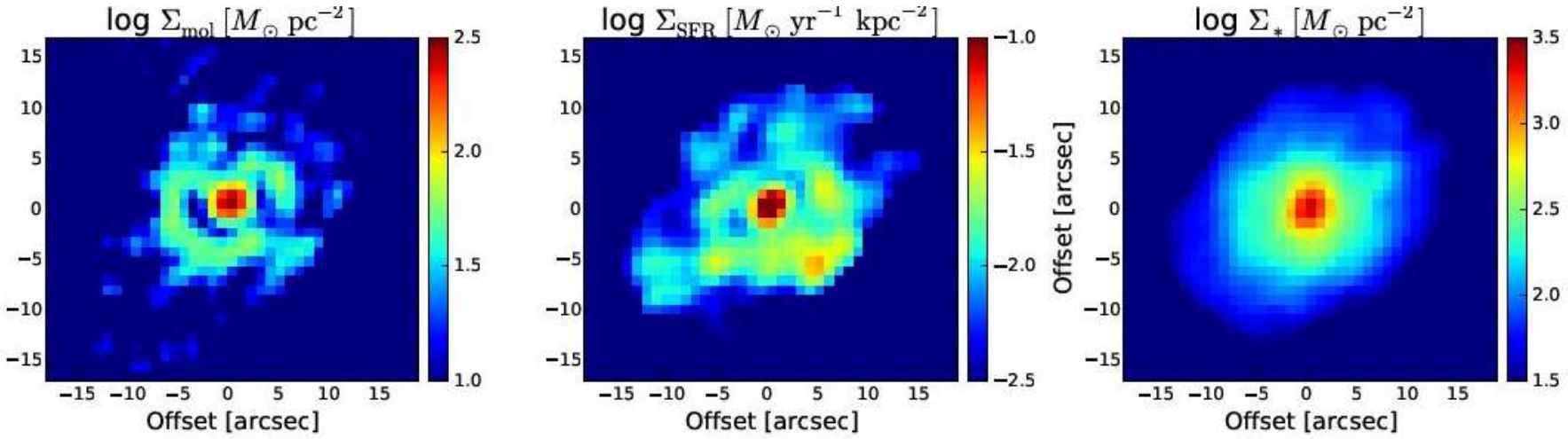

Соотношение Кенникаата-Шмидта и времена исчерпания газа на разных R

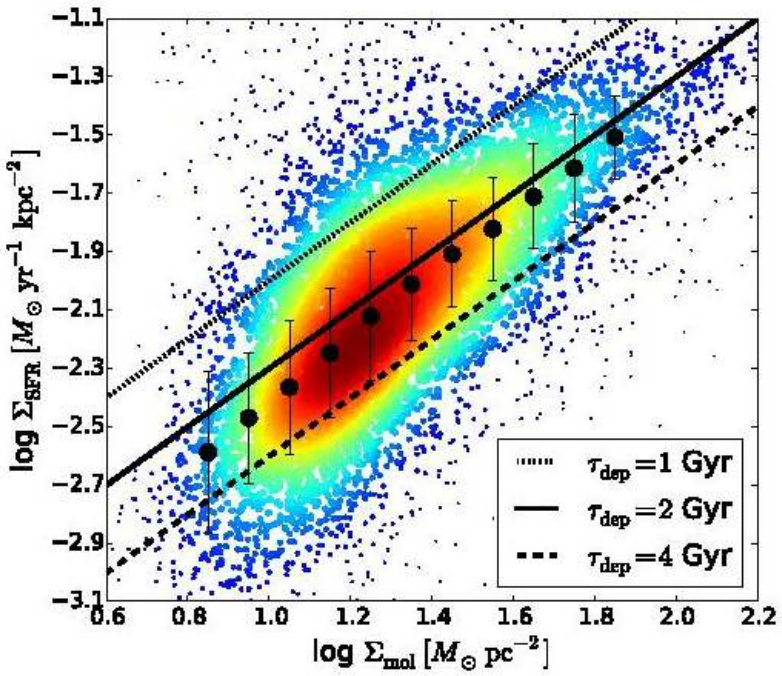

Figure 4. The relationship between $\Sigma_{\rm mol}$ and $\Sigma_{\rm SFR}$ for our sample of 52 galaxies selected from the EDGE survey. The data point plots these values for a $2'' \times 2''$ pixel, with color and point size are coded by the density of data points. The black dots are the median value of $\Sigma_{\rm SFR}$ within bins of $\Sigma_{\rm mol}$. The dotted, solid, and dashed lines correspond to $\tau_{\rm dep}$ = 1, 2, and 4 Gyrs, respectively.

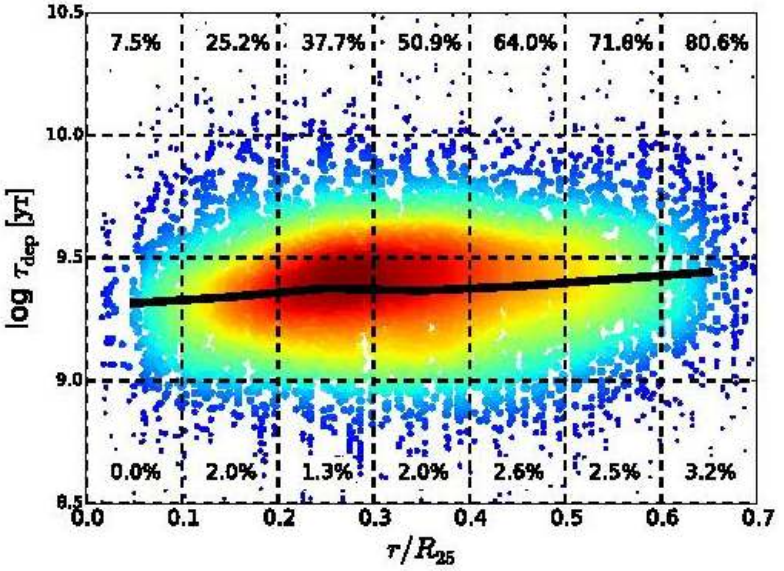

Figure 5. The depletion time as a function of radius, stacked over all detected regions in each sample galaxy. The data points are $2'' \times 2''$ pixel measurements. The colors and sizes of points represent the global density of the data points and the solid line is the median value of $\tau_{\rm dep}$ in a radial bin. On the top and bottom of the figure, we label the fractions of non-detection pixels that correspond to upper and lower limits in $\tau_{\rm dep}$, respectively. Upper limits in $\tau_{\rm dep}$ are pixels with known SFR but CO is not detected, and vice versa for lower limits. The Hα measurements are more sensitive than the CO maps, therefore, the fractions of upper limits are higher than the fractions of lower limits at any radius.

Три типа распределений времени исчерпания по радиусу

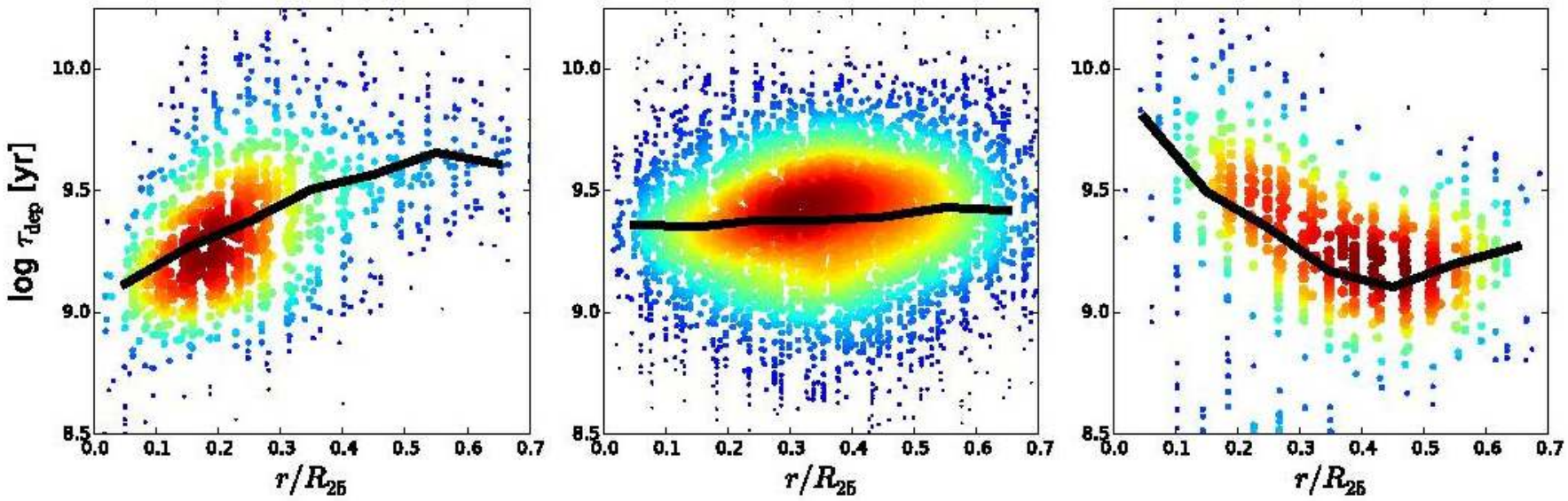

Figure 7. Classifications of $\tau_{\rm dep}$ over detected pixels: galaxies that show a drop of $\tau_{\rm dep}$ in the center (left), similar $\tau_{\rm dep}$ to the disk (middle), and longer $\tau_{\rm dep}$ in the center (right), in relative (top row) and absolute (bottom row) scales. The colors and sizes represent the density of data points. The median profiles for each groups are shown as black curves. The percentages on the top and bottom of top row are the fraction of non-detection, and the number of galaxies in each groups are stated in the bottom right corner of each top panels. This result extends the finding by Leroy et al. (2013), where we show more complex behaviors: galactic centers can have shorter, similar, or longer $\tau_{\rm dep}$ with respect to the disk.

Всякие корреляции

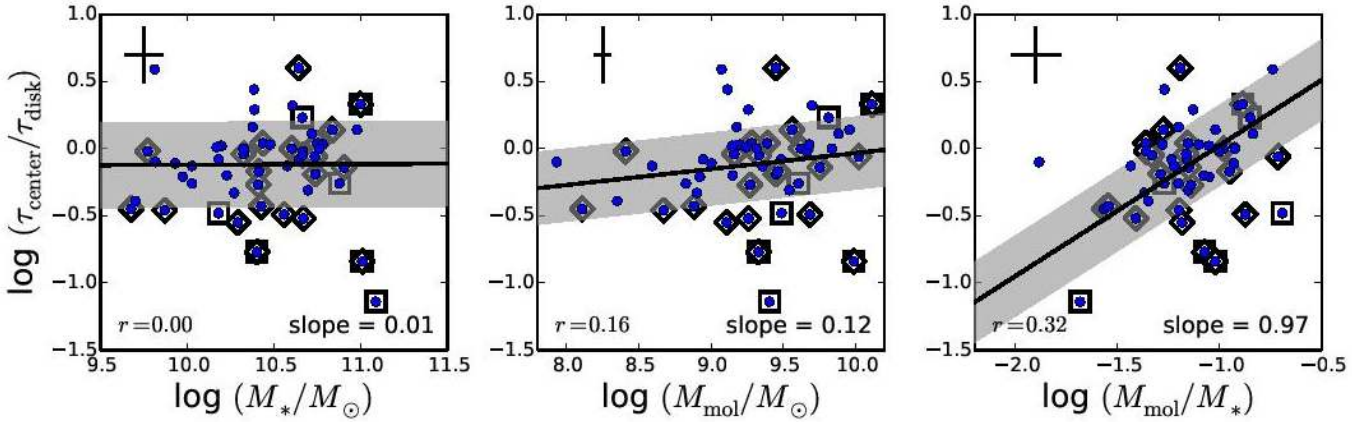

Figure 6. The ratio of $\tau_{\rm dep}$ in a galactic center to that in its disk for each galaxy is plotted as a function of various global parameters: stellar masses (left panel), molecular gas masses (middle panel), molecular-to-stellar mass ratio (right panel). The diamonds mark the barred galaxies, while the squares mark the interacting galaxies. The black lines are the linear best-fit using Orthogonal Distance Regression method in `Scipy` package, which takes into account the errors in both axes, and the gray regions cover 68% of the nearest data points to the best-fit lines. The slope of the best-fit line and the Pearson correlation coefficient are indicated. The crosses represent the typical error bars of the data points.

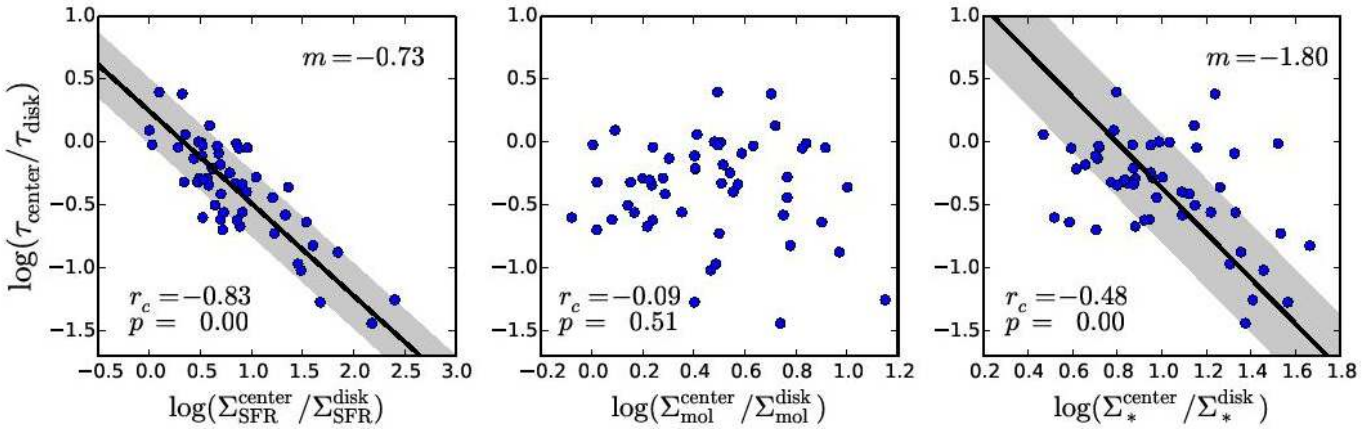

Figure 8. $\tau_{\rm center}$ relative to $\tau_{\rm disk}$ are plotted against Σ_*, $\Sigma_{\rm mol}$, and $\Sigma_{\rm SFR}$, averaged over detected regions in the center (left panel), the disk (middle panel), and the ratio between the two (right panel). The black lines are the linear fit with equal weight using orthogonal distance regression in `Scipy`, and the gray regions cover 68% of data points from the linear fit. The typical uncertainties of the data points are 4 $M_\odot$ pc^{-2} for Σ_* and $\Sigma_{\rm mol}$, and 10^{-4} $M_\odot$ yr^{-1} kpc^{-2} for $\Sigma_{\rm SFR}$. The slope of the correlation (m), the correlation coefficient (r_c), and the p-value (p) are indicated at the corner of each panels. We do not fit the middle panel because of low r_c and high p values, indicative of no correlation between log$(\tau_{\rm center}/\tau_{\rm disk})$ and $\Sigma_{\rm mol}$.

Самая значимая корреляция – с массой галактики?

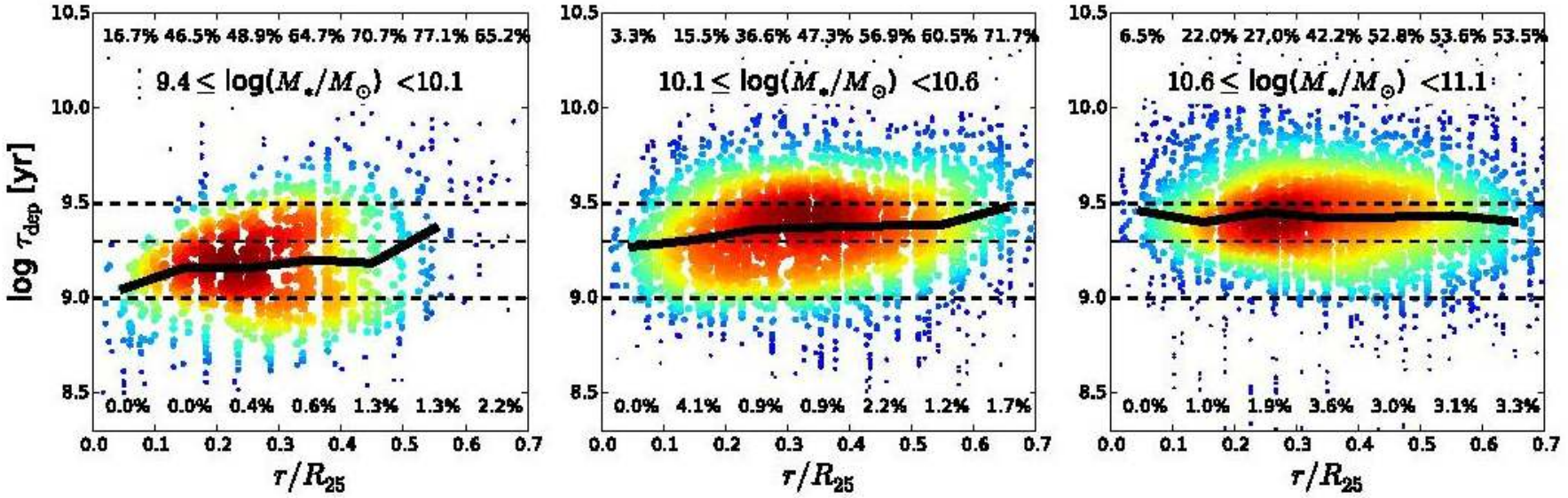

Figure 10. The molecular gas depletion time as a function of radius, separated in three mass bins: $9.6 \leq \log(M_*/M_\odot) < 10.3$ (left panel), $10.3 \leq \log(M_*/M_\odot) < 10.8$ (middle panel), and $10.8 \leq \log(M_*/M_\odot) < 11.3$ (right panel). The colors represent the density of data points. The percentages are the fraction of upper and lower limits at a given radial bin. The solid black lines are the median value of $\tau_{\rm dep}$ at a given radial bin, while the dashed lines are the constant $\tau_{\rm dep}$ values of 1, 2, and 3 Gyrs. This figure shows that the drop of $\tau_{\rm dep}$ in the centers is more prominent in the lowest mass bin.

Диски галактик с эффективным звездообразованием в центре – более компактны

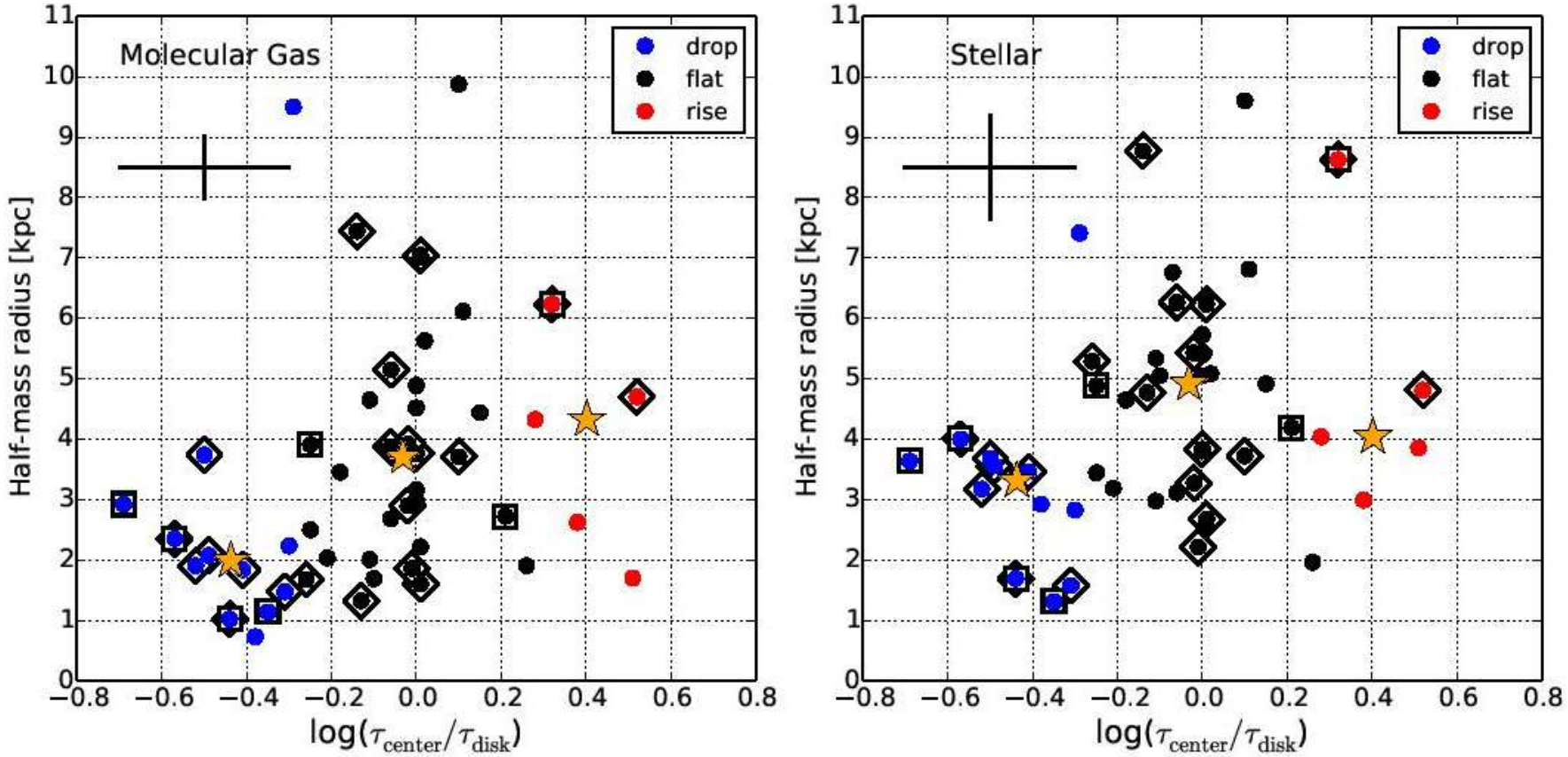

Figure 11. The half-mass radius of molecular gas (left panel) and stars (right panel) for three groups: central drop (blue dots), flat (black dots), and central rise (red dots) of $\tau_{\rm dep}$. The mean values for each three groups are marked as orange stars symbols. The typical errors are shown as crosses. The diamond symbols marked the barred galaxies, while the square symbols marked the interacting galaxies. This shows that the molecular gas distribution in the drop $\tau_{\rm center}$ group and in the disturbed (barred or interacting) galaxies is more compact than those in the other groups.

Но вообще говоря…

- Практически все галактики с коротким временем исчерпания газа в центре – с барами или взаимодействующие; то есть нагнетание газа в центр приводит к более эффективному звездообразованию.

Astro-ph: 1704.03882

AGN ACTIVITY IN NUCLEATED GALAXIES AS MEASURED BY *CHANDRA*

Adi Foord[1], Elena Gallo[1], Edmund Hodges-Kluck[1], Brendan P. Miller[2], Vivienne F. Baldassare[1], Kayhan Gültekin[1], and Oleg Gnedin[1]

Draft version April 14, 2017

ABSTRACT

Motivated by theoretical expectations that Nuclear Star Clusters (NSCs) in galactic centers may provide a favorable environment for super-massive black holes to form and/or efficiently grow, we set out to measure the fraction of nearby nucleated galaxies that also host an Active Galactic Nucleus (AGN). We targeted a distance-limited sample of 98 objects with the *Chandra X-ray Telescope*, down to a uniform X-ray luminosity threshold of $\sim 10^{38}$ erg s^{-1}. The sample is composed of 47 late-types and 51 early-types, enabling us to further investigate the active fraction as a function of galactic morphology. After correcting for contamination to the nuclear X-ray signal from bright X-ray binaries, we measure an active fraction $f = 11.2\%^{+7.4}_{-4.9}$ (1σ C.L.) across the whole sample, in agreement with previous estimates based on an heterogeneous combination of optical, X-ray and radio diagnostics,

Выборка

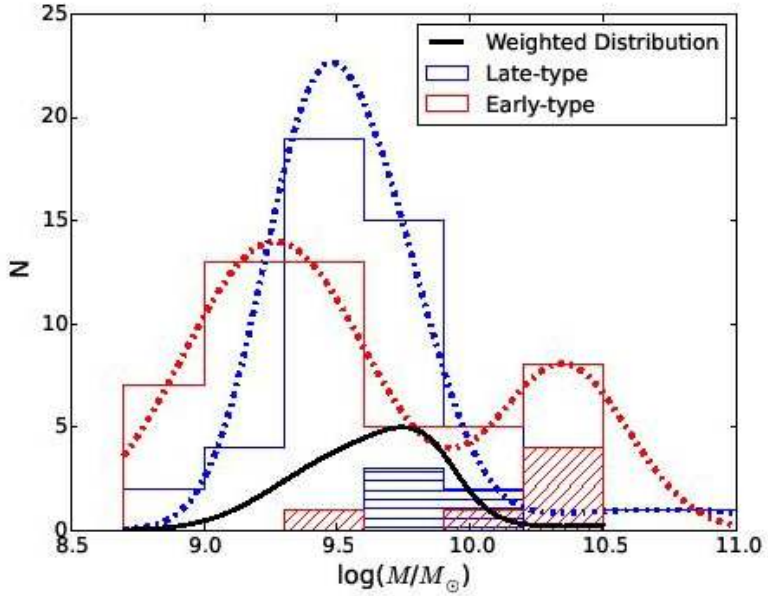

Figure 3. Stellar mass distributions of the late- (open blue histogram) and early-type (open red histogram) samples. The distribution of galaxies with central X-ray detections are shown for both as histograms with diagonal (early-type) and horizontal (late-type) hatching. Each sample has been fit with multiple Gaussians. The weighted distribution, defined as the ratio of the late-type distribution to the early-type distribution, is shown as a black curve. This is used to draw a sub-sample of the early-type galaxies with the same number and mass distribution as the late-type sample,

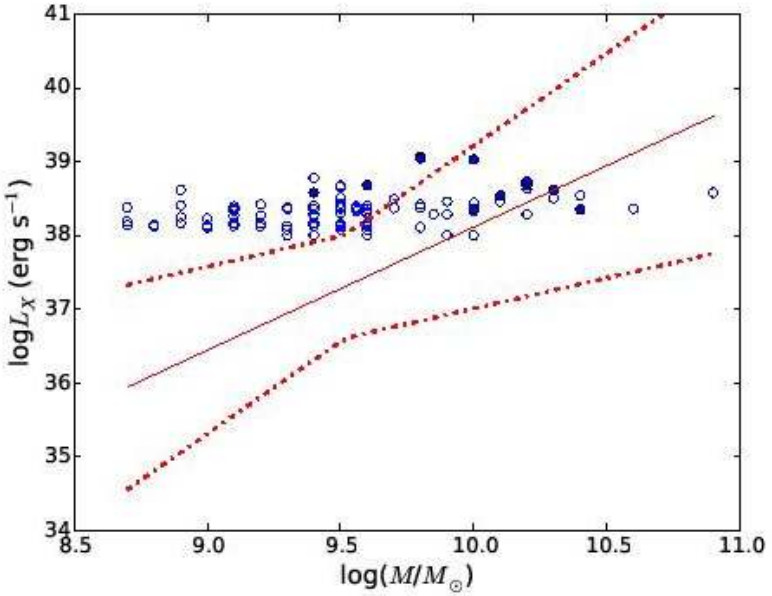

Figure 4. Measured nuclear X-ray luminosities, $L_{\rm X}$, as a function of host galaxy stellar mass, M_*, for our full sample of late and early-type galaxies (98 systems). Filled circles mark detections and open circles mark upper limits. Error bars are taken to be 0.1 dex for both $L_{\rm X}$ and M_*. The "best-fitting relation" from our Bayesian linear regression analysis is shown as a solid red curve, with the dotted lines corresponding to 2σ error bars. Here, 1σ error bars correspond to the 16th and 84th percentiles of the posterior distributions.

Результаты

Table 2
X-ray detections for nucleated late-types

Galaxy (1)	Optical α (J200) (2)	Optical δ (J200) (3)	α (J200) (4)	δ (J200) (5)	δ (6)	X-ray counts (7)
NGC 1042	2:40:23.99	-8:26:01.1	2:40:23.959 (0.12)	-8:26:00.57 (0.12)	0.6	23 (4.8)
NGC 1493	3:57:27.47	-46:12:39.2	3:57:27.454 (0.10)	-46:12:38.55 (0.10)	0.6	48 (6.9)
NGC 4487	12:31:04.48	-8:03:13.8	12:31:04.497 (0.12)	-08:03:12.48 (0.12)	0.8	17 (4.1)
NGC 5879	15:09:46.663	+57:00:00.67	15:09:46.725 (0.08)	+57:00:00.64 (0.08)	0.2	140 (11.8)
NGC 7690	23:33:02.542	-51:41:54.11	23:33:02.528 (0.13)	-51:41:54.44 (0.13)	0.3	17 (4.1)

Note. – Units of right ascension are hours, minutes, and seconds, and units of declination are degrees, arcminutes, and arcseconds. Columns: (1) Galaxy name; (2) and (3): R.A. and Dec. of optical center; (4) and (5): R.A. and Dec. of X-ray nucleus with the positional uncertainty on the centroid position given in parenthesis, in arcseconds; (6) δ between optical center and X-ray nucleus, in arcseconds; (7) nuclear X-ray source net counts extracted between 0.3 and 7 keV, with errors in parenthesis.

Table 3
Nucleated early-type galaxies with X-ray detections

Galaxy (1)	Distance (Mpc) (2)	$\log M_*$ ($\log M_\odot$) (3)	$\log L_X$ ($\log(\mathrm{erg\ s^{-1}})$) (4)
VCC1619	15.49	10.2	38.68
VCC1883	16.60	10.4	38.35
VCC784	15.85	10.3	38.62
VCC1250	17.62	10.2	38.73
VCC1283	17.38	10.1	38.54
VCC1355	16.90	9.4	38.58

Статистика

- Встречаемость активных ядер ВЕЗДЕ около 10% - и в галактиках ранних типов, и в галактиках поздних типов, и в галактиках без ядер, и в галактиках с ядрами

Единственное отличие «хозяев» AGN – более компактные ядра

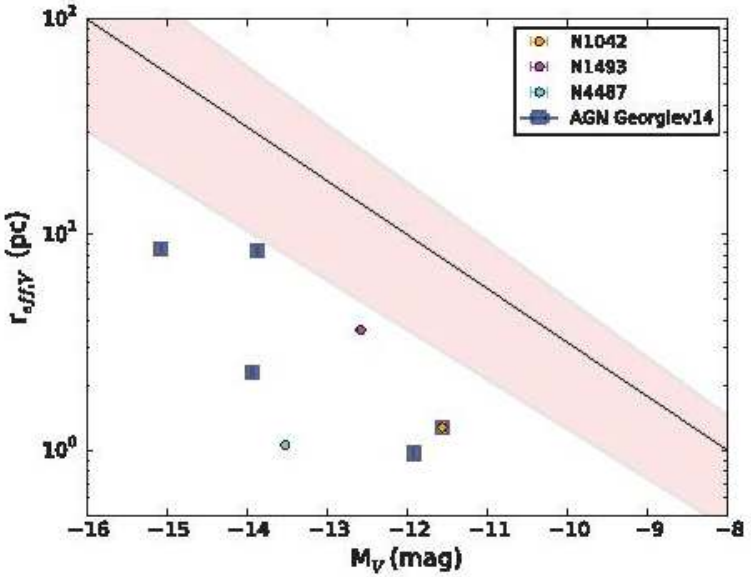

Figure 7. Size-luminosity relation for the NSCs in the catalogue of spiral galaxies analyzed in Georgiev and Böker (2014) is shown in black, with region of error shown in red: log r_{eff} = -2.0±0.2 – 0.25±0.01 M_V. Blue squares denote the galaxies with known AGN in Georgiev and Böker (2014). We add three late-type detections from our sample that are included in their catalogue: NGC 1042 (orange circle with blue square), NGC 1493 (pink circle) and NGC 4487 (cyan circle). NGC 1042 was recognized as an AGN by Georgiev and Böker (2014) but was not included in their compactness study due to S/N < 30 (NGC 1493 and NGC 4487 were excluded from their parent sample for similar reasons). Error bars on M_V are < 0.1 mag. We also find that our nucleated galaxies with AGN tend to have more compact effective radii at a given luminosity.